PHYSICAL REVIEW C VOLUME 18, NUMBER 3 SEPTEMBER 1978

# Neutron emission from actinide muonic atoms

W. W. Wilcke, M. W. Johnson, W. U. Schröder, and J. R. Huizenga
*Deparments of Chemistry and Physics and Nuclear Structure Research Laboratory, University of Rochester, Rochester, New York 14627*

D. G. Perry
*Los Alamos Scientific Laboratory, Los Alamos, New Mexico 87544*
(Received 30 May 1978)

The time distribution of neutrons from radiationless muonic transitions and muon capture has been measured for muonic $^{232}$Th, $^{235}$U, $^{238}$U, $^{237}$Np, $^{239}$Pu, and $^{242}$Pu. Evidence is found for muon capture in fragments from prompt muon-induced fission. Muon-capture rates are deduced and compared to the prediction of the Goulard-Primakoff theory. Isotopic effects of the capture rate are found to be smaller than expected from the systematics. Ratios of $\Gamma_n/\Gamma_f$ are deduced for radiationless transitions. No clear evidence is found for isomeric-state excitation in muonic cascade transitions.

[RADIOACTIVITY Muonic atoms $^{232}$Th, $^{235,238}$U, $^{237}$Np, $^{239,242}$Pu. Measured neutron-time distribution, deduced total muon-capture rates and isotopic effect, $\Gamma_n/\Gamma_f$ ratio for radiationless muonic transitions.]

## I. INTRODUCTION

While a number of groups[1,2] has studied the interactions of negative muons with nuclei of $Z \leq 83$ in recent years, comparatively little is known about muon-induced reactions on the very heaviest nuclei. These heavy muonic atoms are of particular interest for several reasons:

1. Recently developed theories[3-6] on nuclear muon capture predict a strong rate dependence on the neutron excess. Examination of capture rates characteristic of actinide nuclei provides a test of these theories for very neutron-rich nuclei.
2. Since the energies of muonic transitions between the low-lying atomic states[7] are larger than the neutron-binding energies and the fission barriers,[8] radiationless muonic cascade transitions may result in neutron emission or fission in the presence of a bound muon.
3. The presence of the muon itself leads to a perturbation[9,10] of the double-humped fission barrier owing to the muon-nuclear Coulomb interaction.

Information on these subjects may, in principle, be gained by studying any of several processes occurring after a muon stop in the target; for instance, by observing fission fragments emitted following muon capture and subsequent nuclear excitation, or by detecting electrons from the normal leptonic decay of the bound muon. These techniques have been employed by several groups[11-20] in order to deduce muon-capture rates. However, for actinides, such experiments are difficult to interpret owing to the diversity of reaction histories possible with heavy muonic atoms, as pointed out by Bloom[21] and Hadermann.[22]

A sampling of reaction histories possible after the muon has proceeded through the initial stages of its cascade is shown in Fig. 1. Most frequently, muonic x-ray transitions will occur until the muon reaches its $1s$ ground state, whereupon it will either decay or be captured, the latter process causing nuclear fission and/or the emission of neutrons and $\gamma$ rays. In addition, there is a significant probability for radiationless muonic cascade transitions[9,23-26] such as the $2p$-$1s$ or $3d$-$1s$ (Ref. 27) transitions leading to prompt neutron emission or fission followed by the subsequent capture of the muon by a daughter nucleus. Furthermore, as suggested by Błocki *et al.*[10] and Bloom,[21] radiationless transitions may result in a population of shape-isomeric states in the second well of the nuclear potential following yet other reaction channels.

The expected differences in the contributions of the various reaction channels to the total yield of different final products have led Bloom[21] to suggest that the population of isomeric states by radiationless transitions may be inferred from a comparison of muonic lifetimes measured by means of detecting decay electrons and fission fragments. Clearly, a positive identification of such excitation processes would initiate new and interesting nu-

 

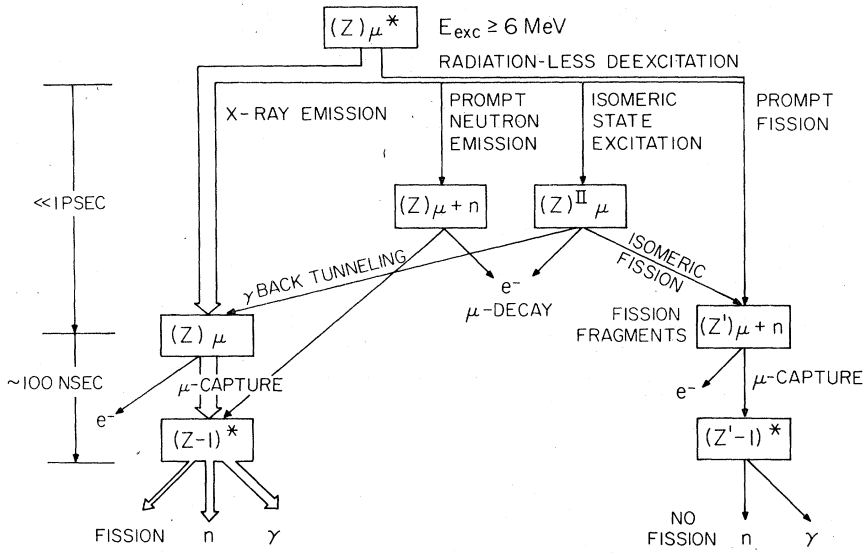


FIG. 1. Simplified diagram of muon-induced reaction channels for actinides. For reasons of clearness, several possible reaction paths have been omitted and products are only identified by their atomic number $Z$.

clear research directed to a study of electromagnetic properties of shape-isomeric states. However, recently Hadermann[22] has argued that possible differences in the experimental lifetimes may be indicative of the muon's history after a prompt fission event. Available data on muon-decay rates[11-13] and muon-induced fission[14-20] are not conclusive in this respect, although some results[19-20] are consistent with isomeric-state excitation in muonic $^{238}$U.

In view of the above discussion, it is obvious that measurements have to be performed to a high accuracy, in order to be able to disentangle the contributions of various reaction channels. Therefore, in this work, neutron emission due to radiationless transitions, muon capture, or muon-induced fission is studied for muonic $^{232}$Th, $^{235,238}$U, $^{237}$Np, and $^{239,242}$Pu. Because subsequent neutron emission is a frequent process in muon-induced reactions and since thick targets can be used, this technique provides muon-capture rates to a higher precision than is easily attainable in decay-electron or fission experiments. As will be shown, coincidence experiments allowing a discrimination against certain reaction channels are feasible employing this method, and the contribution of prompt neutron emission may be assessed. The experimental procedure and the results are presented in the following section. Section III relates to a discussion of the experimental results on muon-capture rates and the importance of prompt neutron emission and fission in muonic actinides.

## II. EXPERIMENTAL PROCEDURE AND RESULTS

The experiments were performed using the LAMPF stopped-muon channel at the Los Alamos Scientific Laboratory. A schematic diagram of the experimental counter array is shown in Fig. 2. Targets were metallic sheets of 5–10 g/cm$^2$ thickness. Incident muons were identified using a four-element plastic counter telescope and a muon stop in the target was defined by the coincidence requirement $123\bar{4}$. A 2.5 cm×12.5 cm diam NE 213 scintillator coupled to an Amperex XP2041Q photomultiplier served as a neutron detector. It was calibrated using standard radioactive $\gamma$ sources. A fast pulse-shape discrimination circuitry (developed and provided by the Hahn-Meitner Institut, Berlin, Germany) provided an efficient (>98%)

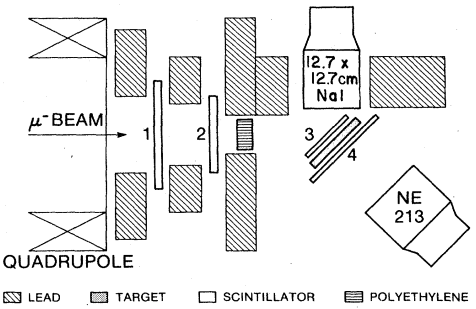


FIG. 2. Schematic diagram of experimental setup. For explanation, see text.

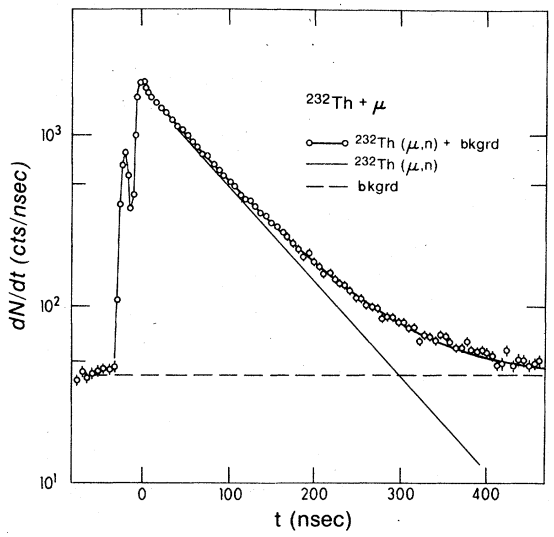


FIG. 3. Part of the experimental neutron-time distribution (points) for muonic $^{232}$Th. The peak in the region near $t = 0$ plotted with higher resolution corresponds to promptly emitted neutrons. The peak on the left side of the distribution is due to $\gamma$-ray events not suppressed by the pulse-shape discrimination. The horizontal dashed line represents the fit of the background distribution adjusted at large positive and negative times with respect to the arbitrarily chosen origin of the $t$ axis. The curve drawn through the data points for positive times represents the total fit to the data, the straight line gives the exponential part of the distribution.

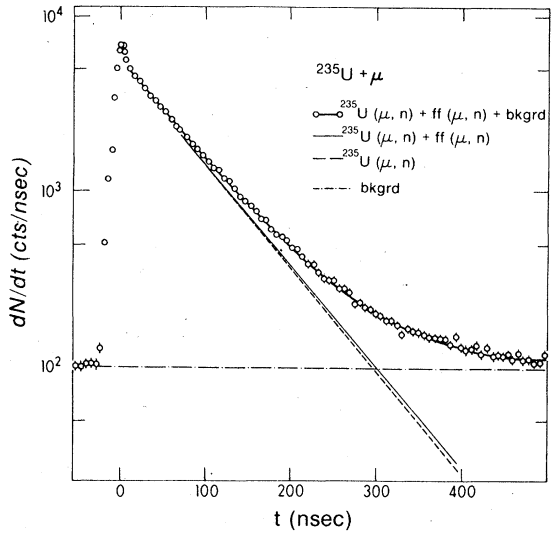


FIG. 4. Neutron-time distribution for muonic $^{235}$U. The solid curve through the data points corresponds to the total fit accounting for muon capture in fission fragments (ff), according to Eq. (3). Otherwise same as Fig. 3.

separation of neutrons from $\gamma$ rays. Fast timing signals generated by a muon-stop event and a neutron signal in the time range between $-200$ and $+800$ nsec with respect to a muon stop were used to start and stop a time-to-amplitude converter, respectively. Typical time resolutions obtained were of the order of 2 nsec for $\gamma$ rays above a threshold of 70 keV. In the case of $^{239}$Pu, a 12.5 cm $\times$ 12.5 cm NaI detector was set up to detect high-energy muonic x rays ($E_x > 6$ MeV), in coincidence with neutrons. In the geometry used, this arrangement provided a coincidence efficiency of 1%. In order to check the time calibration and systematical uncertainties in measurement and data evaluation, a Cu target was used for a test experiment. The measurement yielded $\tau_{Cu} = (163.6 \pm 0.8)$ nsec for the muonic lifetime in Cu, in excellent agreement with the literature value.[28]

Figures 3 to 8 show the important sections of the neutron-time distributions averaged over four to five original channels, as measured for the present six target nuclei. The background measured at negative and large positive delay times with respect to a muon stop turned out to be flat and well describable by a horizontal line as indicated in the figures. Superimposed on this background appears the time distribution of neutrons emitted promptly with respect to a muon stop or delayed after muon capture in a target nucleus or a fission fragment. Neglecting the finite experimental time resolution, the time distribution of the delayed neutrons is given by

$$\frac{dN_d}{dt} = \begin{cases} C\, e^{-\lambda t} F(t), & t \leq t_T \\ C\, e^{-\lambda t} F(t_T), & t \geq t_T, F(t_T) = \text{const}, \end{cases} \tag{1}$$

where $C$ is a constant, $\lambda$ is the total muon-disappearance rate, $t_T$ is the maximum time of flight determined by the energy threshold of the neutron detector and the length $l$ of the flight path. The function $F$ is defined as

$$F(t) = \int_{E(t)}^{\infty} dE' \epsilon(E') \frac{dN_d}{dE'} \exp\left(\lambda \frac{l}{c} \frac{E' + mc^2}{(E'^2 + 2mc^2E')^{1/2}}\right) \tag{2}$$

with $\epsilon(E)$ being the known[29] detection efficiency for a neutron with energy $E$ and $dN_d/dE$ the delayed-neutron energy spectrum. The total time distribution results from the sum of the distribution given by Eq. (1) and the prompt-neutron time-of-flight spectrum $dN_p/dt$ manifesting itself by an additional peak appearing in the time distribution near the arbitrarily chosen origin of the $t$ axis.

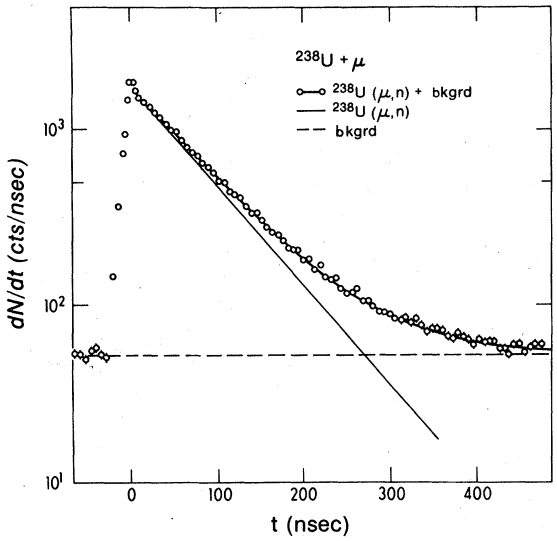


FIG. 5. Same as Fig. 3, but for muonic $^{238}$U.

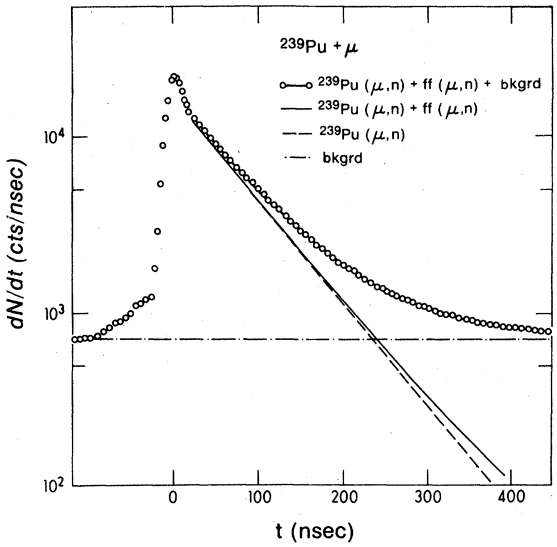


FIG. 7. Same as Fig. 4, but for muonic $^{239}$Pu. The thin solid line includes contributions from muon capture in $^{239}$Pu (dashed line) and fission fragments (ff).

This region is plotted with higher resolution in Figs. 3–8.

In the determination of the muon-disappearance rate $\lambda$, the region affected by the shape of the neutron energy spectrum according to the discussion above, was excluded from the fit. Furthermore, the effect of various muon-induced reactions (cf. Fig. 1) on the time distribution and sources of background were considered.

Following a prompt neutron emission process, the muon may be captured in an isotope of the target element with a rate higher than that corresponding to the target nucleus by an amount $\delta\lambda \sim \Delta\lambda\epsilon_n/(1-\epsilon_n)$. Using an estimated isotopic effect[13] of the capture rates of $\Delta\lambda \approx 4\times10^5$ sec$^{-1}$ and assuming a probability of $\epsilon_n \approx 0.1$ for the above process, one concludes that prompt neutron emission prior to muon capture will influence the deduced capture rate by less than 0.5%, which is statistically insignificant. Similarly, the contamination of the $^{232}$Th neutron-time distribution by $\gamma$-ray events caused by a less efficient pulse-shape discrimination is estimated to have a negligible effect on the deduced capture rate.

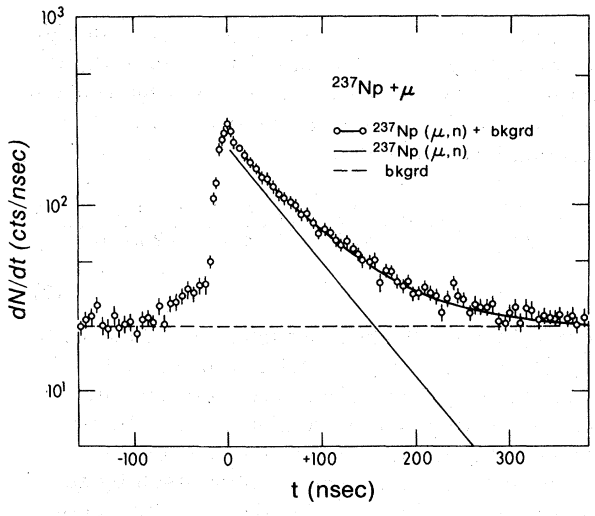


FIG. 6. Same as Fig. 3, but for muonic $^{237}$Np.

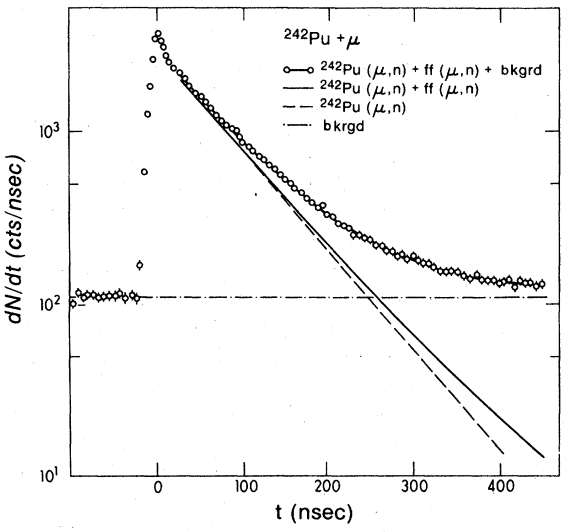


FIG. 8. Same as Fig. 7, but for muonic $^{242}$Pu.

The target materials of $^{235}$U, $^{237}$Np, and $^{239,242}$Pu were clad in 0.1 g/cm$^2$ Cu foil expected to lead to some background in the neutron-time distribution associated with the muonic lifetime in Cu which is about twice as long as that of the actinide targets. From the measured muon-range curve, it is estimated that about 1% of the incident muons may be stopped in the Cu foil. Due to the fact that the multiplicity $M$ of neutrons from muon capture is empirically found[30] to depend on the mass $A$ of the capturing nucleus according to $M \approx 0.3A^{1/3}$ the relative contribution of neutrons from these background events can be estimated to amount to only $\leq 0.5\%$, being smallest in the case of the $^{239}$Pu target.

The statistical accuracy of the present experiments is not high enough to detect the above effect. However, the data clearly indicate the presence of a longer-lifetime component in the neutron-time distribution. This is shown in Fig. 9 exhibiting the background-subtracted time distribution for $^{239}$Pu where the effect is largest. It demonstrates a significant deviation of the data points at large times from an exponential fit applied to the distribution in the region 25 nsec $\leq t \leq$ 250 nsec that is indicated by the dashed line in Fig. 9. These singles data are compared in Fig. 10 with the results of the x-ray neutron coincidence experiment excluding muon-capture events following a high-energy radiationless transition. A constant background has been subtracted from both distributions which

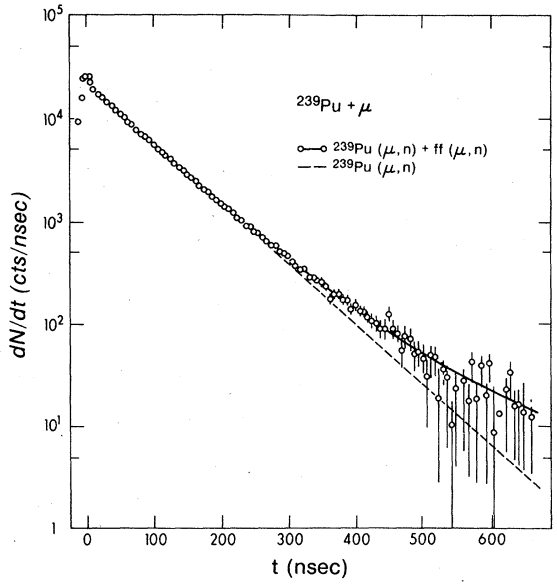


FIG. 9. Background-subtracted neutron-time distribution for muonic $^{239}$Pu. The dashed line represents a fit according to Eq. (3) with $C = n_f = 0$, the full curve represents a fit with $n_f \neq 0$.

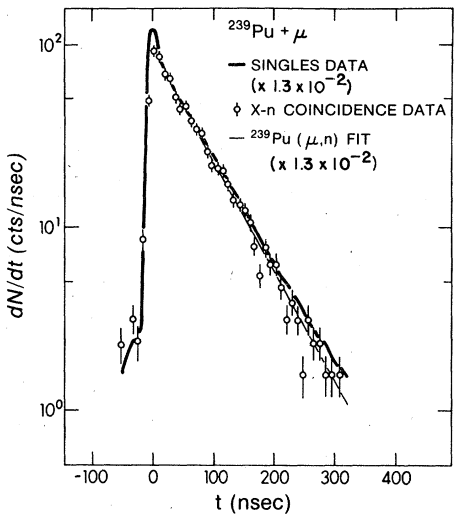


FIG. 10. Background-subtracted singles (solid curve) and x-ray neutron coincidence data (points) normalized to each other, for muonic $^{239}$Pu. The thin line represents a fit corresponding to muon capture in $^{239}$Pu neglecting contributions for fission-fragment muon capture.

are normalized to each other. One notices that the peak of prompt neutrons is absent in the coincidence distribution as expected, since these neutrons are associated with high-energy radiationless cascade transitions. Although the statistical accuracy of the coincidence data is somewhat lower for large delay times, it appears that the data points in this time region lie consistently below the heavy curve representing the singles data. In fact, the coincidence-neutron time distribution is well described by the exponential line obtained from a fit to the singles data at an intermediate time region as indicated by the thin line in Fig. 10. Of course, the coincidence requirement also eliminates background events from the Cu wrapping material, but their contribution is negligibly small, as discussed earlier. From these observations, one is led to conclude that the long-lifetime components of the time distribution, clearly identified also in the cases of $^{235}$U and $^{242}$Pu, are also due to radiationless transition processes followed by muon capture. Prompt neutron emission with subsequent muon capture can be excluded as an origin of these components, because such processes would give rise to shorter lifetimes than the majority of the capture events. This then implies that the effects of muon capture in the fragments from a muon-induced prompt fission process is seen in the neutron-time distributions, as suggested by Hadermann.[22]

Since the statistical accuracy of the present ex-

periments is not high enough to determine independently the muonic lifetimes for the fission fragments, assumptions have to be introduced for these quantities in order to deduce the actinide-muonic capture rates. Radiationless muonic transitions excite an actinide nucleus in a range of excitation energies of magnitude similar to that populated in thermal-neutron capture. From fission systematics,[8] one is then led to adopt a representative value $A_L/A_H = Z_L/Z_H \approx 0.75$ for the mass and charge ratio, respectively, of the two fission fragments produced in a radiationless transition. Assuming one and two neutrons to be evaporated from the light and heavy fragment, respectively, and adopting the systematics[28] of muon-capture rates also for these neutron-rich fragments, average muon lifetimes of $\tau_L \sim 200$ nsec and $\tau_H \sim 120$ nsec are predicted. It is, presently, an interesting but unresolved question, to what extent the muon resides at the light and heavy fragment, respectively, after fission has occurred. For the application in estimating a correction, the ratio of the relative capture probabilities is arbitrarily chosen as $W(Z_H)/W(Z_L) = Z_H/Z_L$.

According to the above discussion, a theoretical function

$$N(t) = C + n_0 \exp(-t/\tau) + n_f[W(Z_H)\exp(-t/\tau_H) + W(Z_L)\exp(-t/\tau_L)] \quad (3)$$

was fitted to that part of the neutron-time distribution not affected by the shape of the neutron energy spectrum, in order to obtain the true muonic lifetimes $\tau = \tau_n^{\mathrm{corr}}$ for the actinides. Here, $C$ denotes the constant background and $n_0$ and $n_f$ are the contributions of neutrons from muon capture in the target nucleus and the fission fragments, respectively. The results of these fits indicated in Figs. 3 to 9 are collected in Table I and compared to those of other techniques. Also included in Table I are values $\tau_n$ for the muonic lifetimes resulting from a fit neglecting the contribution of muon capture by fission fragments, i.e., setting $n_f = 0$ in Eq. (3). The errors quoted include statistical errors and uncertainties of the fit procedure. The assumptions made above concerning the muonic lifetimes for fission fragments may introduce another systematical error of ~1 nsec common to the quoted values for the highly fissionable targets $^{237}$Np and $^{239,242}$Pu, for which the corresponding relative contributions amounted to 2–6%. On the other hand, the consistency of the value $\tau_n^{\mathrm{corr}}$ obtained for $^{239}$Pu by the above procedure with the value $\tau_n$ resulting from the coincidence experiment (cf. Table I) for which no correction is necessary, lends some confidence in this procedure.

The present experiment was not designed to measure the energy spectra of prompt and delayed neutrons. Hence, in order to deduce the physical-

TABLE I. Experimental lifetimes in nsec of muonic actinides deduced from measurements of fission fragments ($\tau_f$), decay electrons ($\tau_e$), capture $\gamma$ rays ($\tau_\gamma$), and neutrons ($\tau_n$). Values $\tau_n^{\mathrm{corr}}$ are obtained from fits to the present data accounting for long-lifetime components (see text). Underlined values correspond to weighted averages.

| Target | $\tau_f$ | $\tau_e$ | $\tau_\gamma$ | $\tau_n$ | $\tau_n^{\mathrm{corr}}$ |
|---|---|---|---|---|---|
| $^{232}$Th | 74.2 ± 5.6 (Ref. 14) | 80.4 ± 2.0 (Ref. 12) | | | |
| | 87.0 ± 4.0 (Ref. 17) | 79.2 ± 2.0 (Ref. 13) | | 80.1 ± 0.6 | |
| | <u>82.7 ± 6.7</u> | <u>79.8 ± 0.6</u> | | | |
| $^{235}$U | 65.3 ± 2.8 (Ref. 16) | 78 ± 4 (Ref. 12) | | | |
| | 66.5 ± 4.2 (Ref. 14) | 75.4 ± 1.9 (Ref. 13) | | 75.0 ± 0.7 | 73.7 ± 0.8 |
| | 75.6 ± 2.3 (Ref. 17) | | | | |
| | <u>70.7 ± 3.4</u> | <u>75.9 ± 1.5</u> | | | |
| $^{238}$U | 75.6 ± 2.9 (Ref. 14) | 88 ± 4 (Ref. 11) | 79.5 ± 0.5 (Ref. 31) | | |
| | 74.1 ± 2.8 (Ref. 16) | 81.5 ± 2.0 (Ref. 12) | 78.6 ± 1.5 (Ref. 20) | 78.3 ± 1.0 | |
| | 76.0 ± 1.0 (Ref. 17) | 73.5 ± 2.0 (Ref. 13) | | | |
| | <u>75.8 ± 0.7</u> | <u>78.7 ± 4.5</u> | <u>79.4 ± 0.6</u> | | |
| $^{237}$Np | 72 ± 2 (Ref. 18) | | | 73.5 ± 1.4 | |
| $^{239}$Pu | 74 ± 14 (Ref. 15) | 77.5 ± 2.0 (Ref. 12) | | | |
| | 70 ± 3 (Ref. 18) | 73.4 ± 2.8 (Ref. 13) | | 74.5 ± 0.5 | 72.6 ± 0.6 |
| | <u>70.2 ± 2.7</u> | <u>76.1 ± 2.2</u> | | 72.9 ± 2.3 [a] | |
| $^{242}$Pu | 79 ± 5 (Ref. 18) | | | 81.1 ± 0.7 | 77.2 ± 1.1 |

[a] X-$n$ coincidence measurement.

ly interesting ratio $n_p/n_d$ of prompt to delayed neutron emission probabilities, information obtained by other workers on the shape of the corresponding spectra is employed. For some heavy elements, it is known[32-35] that both the spectra of delayed[32-34] and prompt[33,35] neutrons are approximately describable by an evaporation shape corresponding to a nuclear temperature parameter $T = 1.2-1.4$ MeV, in a constant-temperature evaporation model. In the analysis, the function determined by Eqs. (1) and (2) and a constant background were subtracted from the neutron-time distribution assuming a delayed neutron energy distribution $dN_d/dE \sim E^{1/2}\exp(-E/T)$ and the calculated[29] detection efficiency $\epsilon$. Assuming the same shape also for the prompt neutrons, the ratio $n_p/n_d$ was determined for a detection threshold of $E_T = 0.5$ MeV. The results are of the order $n_p/n_d = 5-17\%$, as will be discussed below in further detail.

## III. DISCUSSION OF RESULTS

The experimental lifetimes $\tau_n$ of actinide muonic atoms obtained in this work by studying the neutron decay channel are compared in Table I with those resulting from measurements of decay electrons ($\tau_e$), muon-capture $\gamma$ rays ($\tau_\gamma$), and fragments from muon-induced fission ($\tau_f$). In general, the present very accurate muonic lifetimes are consistent with the weighted averages of lifetimes obtained from the other methods. However, for $^{238}$U and $^{239}$Pu, the present uncorrected lifetimes $\tau_n$ are definitely larger than those corresponding to the fission measurements, although the latter show considerable scatter. In the case of $^{239}$Pu, this discrepancy can be ascribed to the effect of muon capture in the fragments produced in a prompt muon-induced fission of the target nucleus, because both the corrected lifetime $\tau_n^{\rm corr}$ as well as the result of the coincidence measurement for $^{239}$Pu agree within the errors with the fission data. This finding supports the suggestion put forward by Hadermann[22] according to which apparent differences of muonic-lifetime measurements can be understood as a manifestation of the muon's fate in a prompt-fission event. However, this effect cannot account for the lifetime difference observed for $^{238}$U because of its smaller prompt-fission probability.[17]

Using the values $\tau_n$ and, where available, $\tau_n^{\rm corr}$ collected in Table I, the experimental muon-capture rates $\lambda_c^{\rm exp}$ can be evaluated according to $\lambda_c^{\rm exp} = 1/\tau_n - R\lambda_0$. Here, $\lambda_0$ is the free-muon decay rate and $R$ (~0.85 for heavy elements) accounts for the reduction of the decay rate due to effects of atomic binding.[36,37] The resulting experimental capture rates are listed in Table II for each target. They are compared with the predictions of the Goulard-Primakoff formula[3]:

$$\lambda_c^{\rm th}(A,Z) = KZ_{\rm eff}^4(\beta)\left(1-\frac{\epsilon_\mu}{m_\mu}\right)^2\left(1-\frac{m_\mu-\epsilon_\mu}{m_N}\right)\times\left[1-0.03\,\frac{A}{2Z}+0.25\,\frac{A-2Z}{2Z}-3.24\left(\frac{A-Z}{2A}+\frac{|A-2Z|}{8ZA}\right)\right]. \quad (4)$$

Here, $K = 272$ sec$^{-1}$ is an overall constant involving the weak-interaction coupling constants, $\epsilon_\mu$ is the muon 1$s$ binding energy, and $m_\mu$ and $m_N$ are the muon and nucleon masses, respectively. The values $Z_{\rm eff}^4(\beta)$, representing the overlap integral of the 1$s$-muon wave function with the nuclear charge distribution, were calculated accounting for the nuclear deformation in a fashion described previously[13] using the parameters[38] listed in Table II. The non-negligible effect of nuclear deformations on the capture rates is demonstrated by the ratio $Z_{\rm eff}^4(\beta)/Z_{\rm eff}^4(0)$ of the overlap integrals correspond-

TABLE II. Experimental muon-capture rates $\lambda_c^{\rm exp}$ compared with the predictions $\lambda_c^{\rm th}$ of the Goulard-Primakoff formula [cf. Eq.(4)]. The half-density radius $c$, the skin thickness $t$, and the deformation parameter $\beta$ of the nuclear charge distribution are given that were used to deduce the overlap integral $Z_{\rm eff}^4(\beta)$.

| Target | $\lambda_c^{\rm exp}$ ($10^7$ sec$^{-1}$) | $c$ (fm) | $t$ (fm) | $\beta$ | $Z_{\rm eff}^4(\beta)$ ($10^6$) | $\frac{Z_{\rm eff}^4(\beta)}{Z_{\rm eff}^4(0)}$ | $\lambda_c^{\rm th}$ ($10^7$ sec$^{-1}$) |
|---|---|---|---|---|---|---|---|
| $^{232}$Th | 1.21 ± 0.01 | 7.10 | 1.49 | 0.230 | 1.407 | 0.966 | 1.10 |
| $^{235}$U | 1.32 ± 0.01 | 7.14 | 1.44 | 0.241 | 1.442 | 0.959 | 1.22 |
| $^{238}$U | 1.24 ± 0.02 | 7.15 | 1.46 | 0.253 | 1.430 | 0.955 | 1.08 |
| $^{237}$Np | 1.32 ± 0.03 | 7.2 [a] | 1.45 [a] | 0.250 [a] | 1.437 | 0.959 | 1.23 |
| $^{239}$Pu | 1.34 ± 0.01 | 7.18 | 1.35 | 0.260 | 1.475 | 0.952 | 1.29 |
| $^{242}$Pu | 1.26 ± 0.02 | 7.2 [a] | 1.45 [a] | 0.250 [a] | 1.464 | 0.955 | 1.16 |

[a] Estimated value.

ing to deformed and spherical nuclear charge distributions, respectively, as shown in Table II.

In comparing the experimental capture rates with the predictions of the Goulard-Primakoff formula [cf. Eq. (4)], it is apparent that the trend of the data is reproduced by the theory, although theoretical capture rates are generally too small. An improved description of the data may be gained by increasing the constant factor in Eq. (4) by ~10%. This, however, would deteriorate the agreement between experiment and theory for the lower-$Z$ elements. The parameters of the deformed nuclear charge distribution listed in Table II, employed in evaluating the overlap integral $Z^4_{\mathrm{eff}}(\beta)$, are subject to some uncertainty. However, these could lead to changes of $Z^4_{\mathrm{eff}}(\beta)$ of the order of only a few percent, whereas the systematic discrepancies between experimental and theoretical values amount to about 10%. Hence, significance has to be assigned to the observed deviation of the theory from the data.

A more stringent test of the Goulard-Primakoff theory can be performed by comparing the experimental isotopic effects of the capture rates to those predicted by Eq. (4), which is possible for the isotope pairs $^{235}$U-$^{238}$U and $^{239}$Pu-$^{242}$Pu. For the relative isotopic differences of the capture rates for two isotopes $A_1$ and $A_2$, $[\lambda_c(A_1, Z) - \lambda_c (A_2, Z)]/\bar{\lambda}_c$, where $\bar{\lambda}_c$ is the mean value of the two rates, one obtains experimentally $(6 \pm 2)\%$ for both the U and Pu cases. It should be noted that the isotopic effect for U can be expected to be slightly smaller in reality than quoted above, because of the unaccounted effect of fission-fragment muon capture for $^{238}$U. In comparision, Eq. (4) yields 12% and 11% for the isotopic effects for the U and the Pu isotopes, respectively.

Although discrepancies between experimental and theoretical capture rates such as discussed above, have also been observed for other elements, it has been argued by Goulard and Primakoff[3] that the coefficients of the various terms in Eq. (4) representing nucleon-nucleon correlation functions should show smaller fluctuations with changing $Z$ and $A$ for the heavier nuclei. However, the systematic and large disagreement between theory and experiment observed in this work for the actinide region, indicates that such an assumption may not be valid, despite the success of the theory for a wide range of elements. It can be hoped that studies of the isotopic effects of muon-capture rates, scarcely performed up to now, may lead to additional insight into the correlations of nucleons in complex nuclei.

Although it has been suggested above that muon capture by a prompt-fission fragment may account for the lifetime differences observed with various techniques, this effect has not been positively identified for $^{238}$U, in the present experiment. In this case, a discrepancy may possibly exist between fission experiments on one hand, and the results of measurements, where decay electrons, capture $\gamma$ rays, or neutrons are detected, on the other hand (cf. Table I). It is, therefore, of interest to examine the predictions of Bloom's model[21] for the rates associated with the neutron and fission channels. In this model, a relative increase of the muon-induced fission rate with respect to those of other channels is expected due to the population of shape-isomeric states by radiationless cascade transitions. Assuming a relative excitation probability $\epsilon$ of such states, the difference between the rates $\lambda_f$ and $\lambda_n$ of fission and neutron emission, respectively, can be calculated following the procedure of Bloom:

$$\lambda_f - \lambda_n = \frac{\epsilon}{\alpha} \frac{\lambda_{if}}{\lambda_c} (\lambda_{if} + \lambda_{bt}) \left(1 - \alpha \frac{\bar{\nu}_{if}}{\bar{\nu}_d}\right). \qquad (5)$$

Here, $\alpha$ denotes the branching ratio of fission following muon capture, $\lambda_{if}$ is the isomeric-fission rate, and $\lambda_{bt}$ is the rate for the system in the second well to tunnel back into the first well. $\bar{\nu}_{if}$ ($\approx 3$) and $\bar{\nu}_d$($\approx 2$) are the average multiplicities of neutrons associated with isomeric fission and muon capture, respectively. Equation (5) is a first-order approximation, valid if $(\lambda_{if} + \lambda_{bt}) \ll \lambda_c$.

Taking the present value for the muon-capture rate of $^{238}$U and the weighted average of the corresponding experimental fission lifetimes (cf. Table I), one calculates a lower limit of $(\lambda_f - \lambda_n) \geq 1.4 \times 10^5$ sec$^{-1}$. With $\alpha = 0.03 \pm 0.007$,[39] $\lambda_{bt} = 5 \times 10^6$ sec$^{-1}$,[40] and $\lambda_{if} = 1.2 \times 10^5$ sec$^{-1}$,[40] Eq. (5) leads to a lower limit for the population of second-well states of $\epsilon \geq 0.09$. This would be consistent with the results of Andert *et al.*,[41] who deduced a probability of ~0.35 for the radiationless $2p$-$1s$ transition in muonic $^{238}$U. However, the above estimate for $\epsilon$ is made using values of $\lambda_{if}$ and $\lambda_{bt}$ corresponding to a nucleus in the absence of a muon. Due to the muon-nuclear Coulomb interaction, one expects[10,21] a relatively smaller decrease of the height of the inner barrier and a larger increase of the outer one, with respect to the second-well ground state. This leads[10] to a reduction of $\lambda_{if}$ by a factor as large as 10 and a slight increase of $\lambda_{bt}$ as compared to the bare-nucleus values. Equation (5) then would predict a much higher value for $\epsilon$ than estimated above, which is physically unrealistic, in particular, as it is known[25-27,34] and confirmed by this experiment that direct neutron emission is a process of major importance in radiationless transitions. Furthermore, charged-particle induced reactions yield values of only $10^{-5}$ to $10^{-4}$ for $\epsilon$.[40] Hence, there is presently no plausible ex-

planation for the large rate difference observed for $^{238}$U. High-precision fission and $X$-$n$ coincidence experiments are needed to settle this question.

A rather interesting quantity pertaining to the interaction of muons with actinide nuclei is the ratio $\Gamma_n/\Gamma_f$ of the probabilities for neutron emission and fission, respectively, associated with a radiationless transition leading to excitation energies close to the perturbed fission barrier. This ratio is connected to the ratio $n_p/n_d$ of prompt-to-delayed neutron emission determined in this work. The measured intensity $n_d$ of delayed neutrons can be written as $n_d = \Omega\bar{\nu}_d$, where $\bar{\nu}_d$ is the average neutron multiplicity associated with one muon-capture event and $\Omega$ is a factor containing solid angle, efficiency of the detection system, and the number of muons stopped in the target. The number of promptly emitted neutrons is given by $n_p \approx \Omega(P_{pf}\bar{\nu}_{pf} + \nu_{dir})$, where $P_{pf}$ is the probability per muon stop for prompt fission, $\bar{\nu}_{pf} \approx 3$ is the average multiplicity of neutrons emitted in this process,[8] and $\nu_{dir}$ is the probability for a neutron to be directly emitted in a radiationless transition. One then obtains

$$\frac{n_p}{n_d} \approx \frac{P_{pf}\bar{\nu}_{pf} + \nu_{dir}}{\bar{\nu}_d} \tag{6}$$

and, inserting the identity $\Gamma_n/\Gamma_f = \nu_{dir}/P_{pf}$,

$$\frac{\Gamma_n}{\Gamma_f} \approx \frac{n_p}{n_d}\frac{\bar{\nu}_d}{P_{pf}} - \bar{\nu}_{pf}\,. \tag{7}$$

Similarly, the multiplicity $\bar{\nu}_d$ of delayed neutrons contains contributions from both muon capture and the deexcitation of fragments from muon-capture-induced fission. The relative contribution of the latter process was estimated taking values of $\Gamma_n/\Gamma_f$ for various isotopes from the literature[8] and determining the probabilities of first-, second-, and third-change fission employing a Monte Carlo method. The mean initial excitation energy ($E^*$ ~15–20 MeV) due to the muon-capture process, as well as the neutron multiplicity in the number of cases not leading to fission were calculated more accurately employing Singer's model,[30,34] which is able to describe consistently muon-capture neutron multiplicities for a wide range of target elements. A temperature parameter of $T \sim 1.4$ MeV was assumed in the calculations as discussed earlier. Systematic uncertainties of ~30% have to be assigned to the evaluated quantities $\bar{\nu}_d$.

Experimental values for $n_p/n_d$ and the theoretical multiplicities $\bar{\nu}_d$ are collected in Table III. The experimental prompt-fission probabilities $P_{pf}$ from other workers show considerable scatter. The values adopted in Table III represent recent measurements[17,18] of $P_{pf}$ covering the nuclides of interest. They allow to compare $\Gamma_n/\Gamma_f$ ratios as deduced from Eq. (7) at least for the two U and Pu isotope pairs, since it can be expected that systematic errors in the above procedure compensate in such a comparison.

TABLE III. Experimental ratios $n_p/n_d$ of prompt and delayed neutron emission probabilities and the deduced ratios $\Gamma_n/\Gamma_f$ of the probabilities for neutron emission and fission for radiationless transitions. $P_{pf}$ is the probability for muon-induced prompt fission. The multiplicity $\bar{\nu}_d$ of neutrons associated with muon capture has been derived as described in the text. Uncertainties of ~30% have to be assigned to the $\Gamma_n/\Gamma_f$ values.

| Target | $n_p/n_d$ | $P_{pf}$ | $\bar{\nu}_d$ | $\Gamma_n/\Gamma_f$ |
|---|---|---|---|---|
| $^{232}$Th | 0.049 | $(5.0 \pm 1.2)\times10^{-4}$(Ref. 17) | 1.9 | 180 |
| $^{235}$U | 0.11 | $(5.1 \pm 1.2)\times10^{-3}$(Ref. 17) | 2.4 | 48 |
| $^{238}$U | 0.08 | $(2.03 \pm 0.45)\times10^{-3}$(Ref. 17) | 2.2 | 83 |
| $^{239}$Pu | 0.14 | 0.015(Ref. 18) | 3.1 | 25 |
| $^{242}$Pu | 0.17 | 0.038(Ref. 18) | 2.8 | 9 |

Some qualitative observations can be made from the resulting $\Gamma_n/\Gamma_f$ values for radiationless transitions, which are listed in Table III: Beyond all systematic uncertainties involved in the present derivation of $\Gamma_n/\Gamma_f$, these ratios for muonic actinides are significantly higher than similar values for the bare nuclei obtained from charged-particle induced fission[42,43] or photofission reactions[18,44] at excitation energies slightly above the neutron binding energy. For example, $\Gamma_n/\Gamma_f$ for the two muonic U isotopes is increased by a factor of ~30 as compared to the ratio resulting from particle-induced reactions[42,43] and is larger by factors ~10 compared to the $(\gamma,f)$ values.[18,44] Such a comparison has to be made with caution, however, since the height and shape of the fission barrier depends on the nature of the transition state through which the fissioning nucleus proceeds. Whereas particle-induced reactions can populate[42,43] states of even-even nuclei at saddle-point deformation that are similar to those of the ground-state vibrational band ($K^\pi = 0^+$), the $\gamma$-vibrational band ($K^\pi = 0^-$, $1^-$, and $2^-$), photoabsorption is generally a much simpler process. Excitation by radiationless muonic transitions can be expected to be closely related to photoabsorption, because both processes are characterized by dominant electric dipole ($E1$) and quadrupole ($E2$) transitions. However, whereas it is known[44] that $E1$ excitation is dominant in photoabsorption, the relative strengths of $E1$ and $E2$ radiationless transitions are not well known. Nevertheless, the significant increase of the muonic $\Gamma_n/\Gamma_f$ ratios over the corresponding values

from the $(\gamma,f)$ reactions provides strong evidence for an increase of the fission barriers in the presence of the muon, as suggested by Błocki *et al.*[10] Of similar significance is the stronger dependence of the muonic $\Gamma_n/\Gamma_f$ value on the fissibility than that observed with the other reactions. A further discussion of the present results has to await an improved knowledge of the excitation function corresponding to radiationless muonic cascade transitions. Precise measurements of the missing x-ray intensities and the prompt-neutron energy spectra from muonic actinides would be of considerable importance in this respect.

The authors would like to express their gratitude to J. L. Smith and C. Longmire (LASL) for supplying the target material. Thanks are due J. C. Browne, S. D. Bloom (LLL), and W. K. Hensley (LASL) for their help during the data acquisition and valuable discussions. The hospitality and assistance of the LAMPF technical staff are noted with appreciation. This work was supported by the U.S. Department of Energy.

[1]*Muon Physics*, edited by C. S. Wu and V. Hughes (Academic, New York, 1975), and references cited therein.
[2]R. Engfer, H. Schneuwly, J. L. Vuilleumier, H. K. Walter, and A. Zehnder, At. Data Nucl. Data Tables 14, 509 (1974), and references cited therein.
[3]B. Goulard and H. Primakoff, Phys. Rev. C 10, 2034 (1974).
[4]B. Goulard, J. Joseph, and F. Ledoyen, Phys. Rev. Lett. 27, 1238 (1971).
[5]J. Joseph, F. Ledoyen, and B. Goulard, Phys. Rev. C 6, 1742 (1972).
[6]A. Mekjian, Phys. Rev. Lett. 36, 1242 (1976).
[7]K. W. Ford and J. G. Wills, Nucl. Phys. 35, 295 (1962).
[8]R. Vandenbosch and J. R. Huizenga, *Nuclear Fission* (Academic, New York, 1973).
[9]D. F. Zaretsky and V. M. Novikov, Nucl. Phys. 28, 177 (1961).
[10]J. Błocki, Z. Sujkowski, and M. Zielińska-Pfabé, Phys. Lett. 42B, 415 (1972).
[11]J. C. Sens, Phys. Rev. 113, 679 (1959).
[12]O. Hashimoto, S. Nagamiya, K. Nagamine, and T. Yamazaki, Phys. Lett. 62B, 233 (1976).
[13]M. W. Johnson, W. U. Schröder, J. R. Huizenga, W. K. Hensley, D. G. Perry, and J. C. Browne, Phys. Rev. C 15, 2169 (1977).
[14]J. A. Diaz, S. N. Kaplan, and P. V. Pyle, Nucl. Phys. 40, 54 (1963).
[15]V. Cojucaru, L. Marinescu, M. Petrascu, G. Voiculescu, A. Ignatenko, and M. Omelianenko, Phys. Lett. 20, 53 (1966).
[16]B. Budick, S. C. Cheng, E. R. Macagno, A. M. Rushton, and C. S. Wu, Phys. Rev. Lett. 24, 604 (1970).
[17]D. Chultem, V. Cojocaru, Dz. Ganzorig, Kim Si Chwan, T. Krogulski, V. C. Kuznetsov, H. G. Ortlepp, S. M. Polikanov, B. M. Sabirov, U. Schmidt, and W. Wagner, Nucl. Phys. A247, 452 (1975).
[18]B. M. Aleksandrov, G. V. Buklanov, W. D. Fromm, Dz. Ganzorig, A. S. Krivokhatski, T. Krogulski, S. M. Polikanov and B. M. Sabirov, Phys. Lett. 57B, 238 (1975).
[19]Dz. Ganzorig, P. G. Hansen, T. Johansson, B. Jonson, J. Konijn, T. Krogulski, V. D. Kuznetsov, S. M. Polikanov, G. Tibell, and Z. Westgaard, Contribution Q12 to Seventh International Conference on High Energy Physics and Nuclear Structure, Zurich, 1977 (unpublished).
[20]W. D. Fromm, H. G. Ortlepp, S. M. Polikanov, U. Schmidt, G. N. Zorin, R. Arlt, and G. Musiol, Nucl. Phys. A278, 387 (1977).
[21]S. D. Bloom, Phys. Lett. 48B, 470 (1974); UCRL Report No. UCRL-76974, 1975 (unpublished).
[22]J. Hadermann, Phys. Lett. 67B, 35 (1977).
[23]D. F. Zaretsky, in Proceedings of the Second United Nations International Conference on Peaceful Uses of Atomic Energy, Geneva, 1958 (unpublished), Vol. 15, p. 175.
[24]D. F. Zaretsky and V. M. Novikov, Nucl. Phys. 14, 540 (1960).
[25]V. Srinivasan and M. K. Sundaresan, Can. J. Phys. 49, 621 (1971).
[26]K. P. Lohs, G. Wolschin, and J. Hüfner, Nucl. Phys. A236, 457 (1974).
[27]H. Schneuwly, L. Schellenberg, H. Backe, R. Engfer, U. Jahnke, E. Kankeleit, K. H. Lindenberger, R. M. Pearce, C. Petitjean, W. U. Schröder, H. K. Walter, and A. Zehnder, Nucl. Phys. A196, 452 (1972).
[28]M. Eckhause, R. T. Siegel, R. E. Welsh, and T. A. Filipas, Nucl. Phys. 81, 525 (1966).
[29]R. E. Textor and V. V. Verbinski, ORNL Report No. ORNL-4160, 1968 (unpublished).
[30]P. Singer, in *Springer Tracts in Modern Physics* (Springer, New York, 1974), Vol. 71, p. 39.
[31]S. N. Kaplan, J. A. Monard, and S. Nagamiya, Phys. Lett. 64B, 217 (1976).
[32]V. S. Evseev and T. N. Mamedov, Yad. Fiz. 19, 1222 (1974) [Sov. J. Nucl. Phys. 19, 624 (1974)]; Yad. Fiz. 18, 968 (1973) [Sov. J. Nucl. Phys. 18, 499 (1974)].
[33]V. S. Evseev, T. Kozłowski, T. Mamedov, V. S. Roganov, Z. Sujkowski, J. Wojtkowska, and A. Zgliński, in *Proceedings of the International Conference on Photonuclear Reactions and Applications, Asilomar*, 1973, edited by B. L. Berman (Univ. of California, AEC publication, 1973), p. 641.
[34]W. U. Schröder, Report No. IKDA 73/17, 1973 (unpublished); W. U. Schröder, U. Jahnke, K. H. Lindenberger, G. Röschert, R. Engfer, and H. K. Walter, Z. Phys. 268, 57 (1974).
[35]C. K. Hargrove, E. P. Hincks, G. R. Mason, R. J. McKee, D. Kessler, and S. Ricci, Phys. Rev. Lett. 23, 215 (1969).
[36]R. W. Huff, Ann. Phys. (N.Y.) 16, 288 (1961).
[37]I. M. Blair, H. Muirhead, T. Woodhead, and J. N. Woulds, Proc. Phys. Soc. 80, 938 (1962).
[38]S. A. de Wit, G. Backenstoss, C. Daum, J. C. Sens, and H. L. Acker, Nucl. Phys. 87, 657 (1967).
[39]J. Hadermann and K. Junker, Nucl. Phys. A256, 521

(1976).
[40]P. A. Russo, J. Pedersen, and R. Vandenbosch, Nucl. Phys. A240, 13 (1975).
[41]K. Andert, R. Arlt, D. Chultem, V. Cojocaru, Dz. Ganzorig, V. S. Evseev, B. Hahn, H. Haupt, A. I. Kalinin, T. Krogulski, N. Nenoff, H. G. Ortlepp, S. M. Polikanov, B. M. Sabirov, and U. Schmidt, in *Proceedings of the International Conference on Nuclear Physics, Munich, 1973,* edited by J. de Boer and J. J. Mang (North-Holland, Amsterdam, 1973), p. 609.
[42]B. B. Back, O. Hansen, H. C. Britt, and J. D. Garrett, Phys. Rev. C 9, 1924 (1974).
[43]B. B. Back, H. C. Britt, O. Hansen, B. Leroux, and J. D. Garrett, Phys. Rev. C 10, 1948 (1974).
[44]L. J. Lindgren and A. Sandell, Z. Phys. A 285, 415 (1978).